JOC The Journal of Organic Chemistry

Article

pubs.acs.org/joc

DFT Investigation on Mechanisms and Stereoselectivities of [2 + 2 + 2] Multimolecular Cycloaddition of Ketenes and Carbon Disulfide Catalyzed by N-Heterocyclic Carbenes

Wen-Jing Zhang, Dong-Hui Wei,* and Ming-Sheng Tang*

The College of Chemistry and Molecular Engineering, Zhengzhou University, Zhengzhou, Henan Province 450001, People's Republic of China

Supporting Information

ABSTRACT: The first theoretical investigation using density functional theory (DFT) methods to study the detailed reaction mechanisms of stereoselective [2 + 2 + 2] multimolecular cycloaddition of ketene (two molecules) and carbon disulfide (CS_2, one molecule) which is catalyzed by N-heterocyclic carbene (NHC) is presented in this paper. The calculated results indicate that this reaction occurs through four steps: the complexation of NHC with ketene (channel 1a) rather than with CS_2 (channel 1b), addition of CS_2 (channel 2b) but not dimerization of ketene (channel 2a), formal [4 + 2] cycloaddition with a second molecule of ketene (channel 3a) rather than intramolecular [2 + 2] cycloaddition (channel 3b), and finally regeneration of NHC. The second step is revealed to be the rate-determining step. Moreover, the stereoselectivities associated with the chiral carbon center and the carbon double bond are predicted to be respectively determined in the second and third steps and respectively *R* and *E* configurations dominated, which are in good agreement with the experimental results. Furthermore, the possible mechanisms of the identical [2 + 2 + 2] cycloaddition catalyzed by *N*,*N*-dimethylpyridin-4-amine (DMAP) have also been investigated to help understand the ring closure mechanism proceeding in the third step.

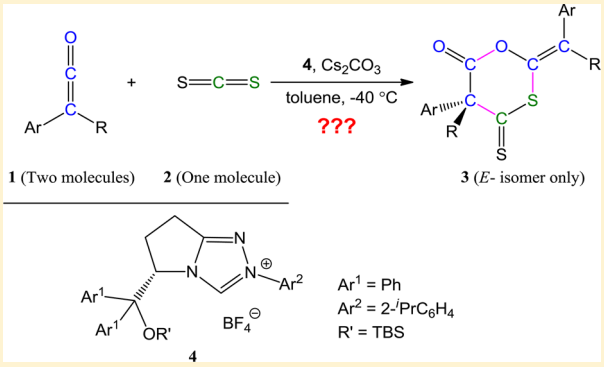

1. INTRODUCTION

During the past decades, N-heterocyclic carbenes (NHCs) have been found to be a key variety of compounds working as the ligands of organometallic catalysts[1,2] and Lewis base organocatalysts.[3−5] One of the most important successes in the latter applications is the use of NHCs as powerful organocatalysts for ketene cycloaddition reactions with high stereoselectivities, which affords a facile and also effective way to obtain various heterocyclic complexes.[6−11]

Carbon disulfide (CS_2) is frequently used in organic chemistry as an attractive C_1 building block for the synthesis of sulfur-containing organic complexes,[12,13] especially for the rapid construction of sulfur heterocycles.[14,15] Although cycloadditions with CS_2 that are catalyzed by Lewis bases[16−19] or organometallic compounds[20,21] have been widely reported, the recent work of Ye and co-workers[10] on NHC-catalyzed [2 + 2 + 2] cycloaddition of ketene (two molecules) with CS_2 (one molecule) deserves particular attention if we note the fact that this is the first enantioselective catalytic cycloaddition of CS_2.

Scheme 1 illustrates more experimental details of this multimolecular cycloaddition: two molecules of ketene **1** react with one molecule of CS_2 **2** to afford the six-membered (sulfur, oxygen) heterocyclic compound **3**, catalyzed by NHC **4′** (generated from the triazolium salt **4** by eliminating a molecule of HBF_4) at −40 °C using toluene as the solvent. The

Scheme 1. Experimental Details of the Title Reaction

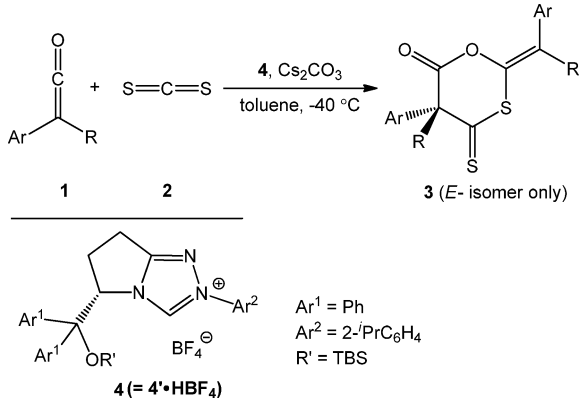

ee values range from 92% to 97% according to different substituent groups of ketene, and only the *E* isomer of product **3** is detected in the experiment. Ye and co-workers have also conducted some efforts to propose the possible catalytic mechanism, and a definite conclusion is drawn through their

Received: August 26, 2013
Published: November 4, 2013

Scheme 2. Proposed Reaction Mechanism of the Title Reaction Catalyzed by Cata

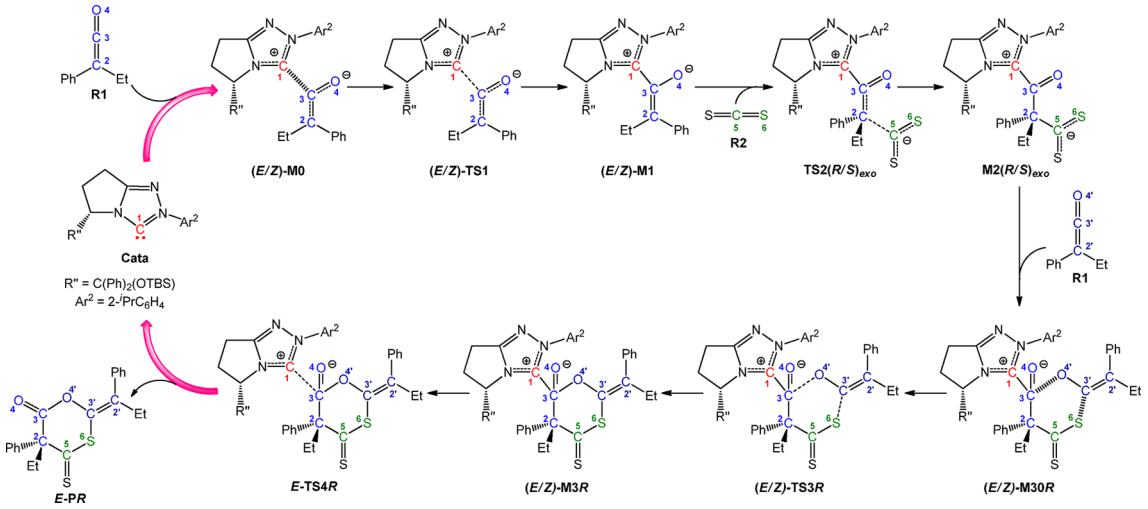

Scheme 3. Possible Reaction Mechanisms for Each Elementary Step using Cata as the Catalyst

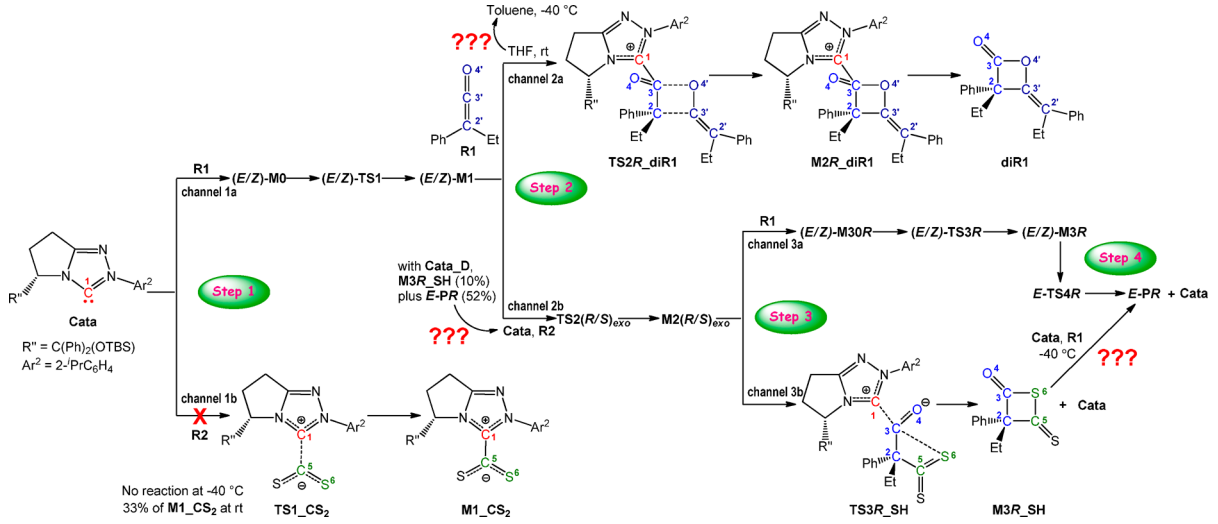

control experiments—the initial step of the reaction is addition of NHC to ketene rather than to CS_2. Their explorations for other remaining steps are quite instructive, but there are some key issues that are ambiguous.

For the sake of convenience, we will introduce some abbreviations in the rest of this paper; in particular, we will denote the NHC catalyst **4′** as **Cata**, the phenyl(ethyl)ketene (i.e., Ar = Ph and R = Et), which is chosen as the representation of ketene since it is reported to react with CS_2 by affording excellent yield (99%) and enantioselectivity (96%), as **R1**, and the carbon disulfide as **R2**.

As we all know, for a multimolecular reaction, it is crucial to make clear which molecules are involved in each elementary step (far beyond the initial one only) in order to access a complete understanding of the reaction mechanisms. On the basis of the presumption suggested by Ye[10] and our previous theoretical studies on the mechanisms of NHC-catalyzed ketene [2 + 2][22] and [4 + 2][23] cycloaddition reactions, we propose a possible catalytic cycle for the title stereoselective [2 + 2 + 2] multimolecular cycloaddition and illustrate it in Scheme 2: there are generally four steps in this cycle, including (1) the combination of ketene **R1** with **Cata**, where *exo* and *endo* attacks are possible to occur to form the two precursor complexes (*E*/*Z*)-**M0** (synonymous with *E*-**M0** and *Z*-**M0**, and similarly hereafter), respectively, and then the adducts (*E*/*Z*)-**M1** are generated via transition states (*E*/*Z*)-**TS1** separately, (2) the reaction between adducts *E*-**M1** and **R2** to give intermediates **M2**$(R/S)_{exo}$ via transition states **TS2**$(R/S)_{exo}$, respectively, where the reaction of *Z*-**M1** with **R2** is left out because we suppose it to be unfavorable,[22] (3) the [4 + 2] cycloaddition of **M2**R_{exo} with a second molecule of **R1** to form the precursor complexes (*E*/*Z*)-**M30***R* and then further to (*E*/*Z*)-**M3***R* via transition states (*E*/*Z*)-**TS3***R* separately, with the reaction of **M2**S_{exo} with **R1** being excluded as it is also considered to be energetically unfavorable,[10] and (4) the regeneration of **Cata**.

Nevertheless, there is more than one possible reaction mechanism for each of the first three steps according to diverse literature reports. We created a brief summation and illustrated them in Scheme 3. For the first step, it is not easy to figure out whether **Cata** interacts with **R1** through channel 1a or with **R2** through channel 1b to initiate the reaction, because one may get diverse answers according to the specific structures of the NHCs, the counterpart reactants, and also the specific experimental conditions such as temperature or solvent. In our aforementioned theoretical study on ketene [2 + 2]

dx.doi.org/10.1021/jo4018809 | J. Org. Chem. 2013, 78, 11849−11859

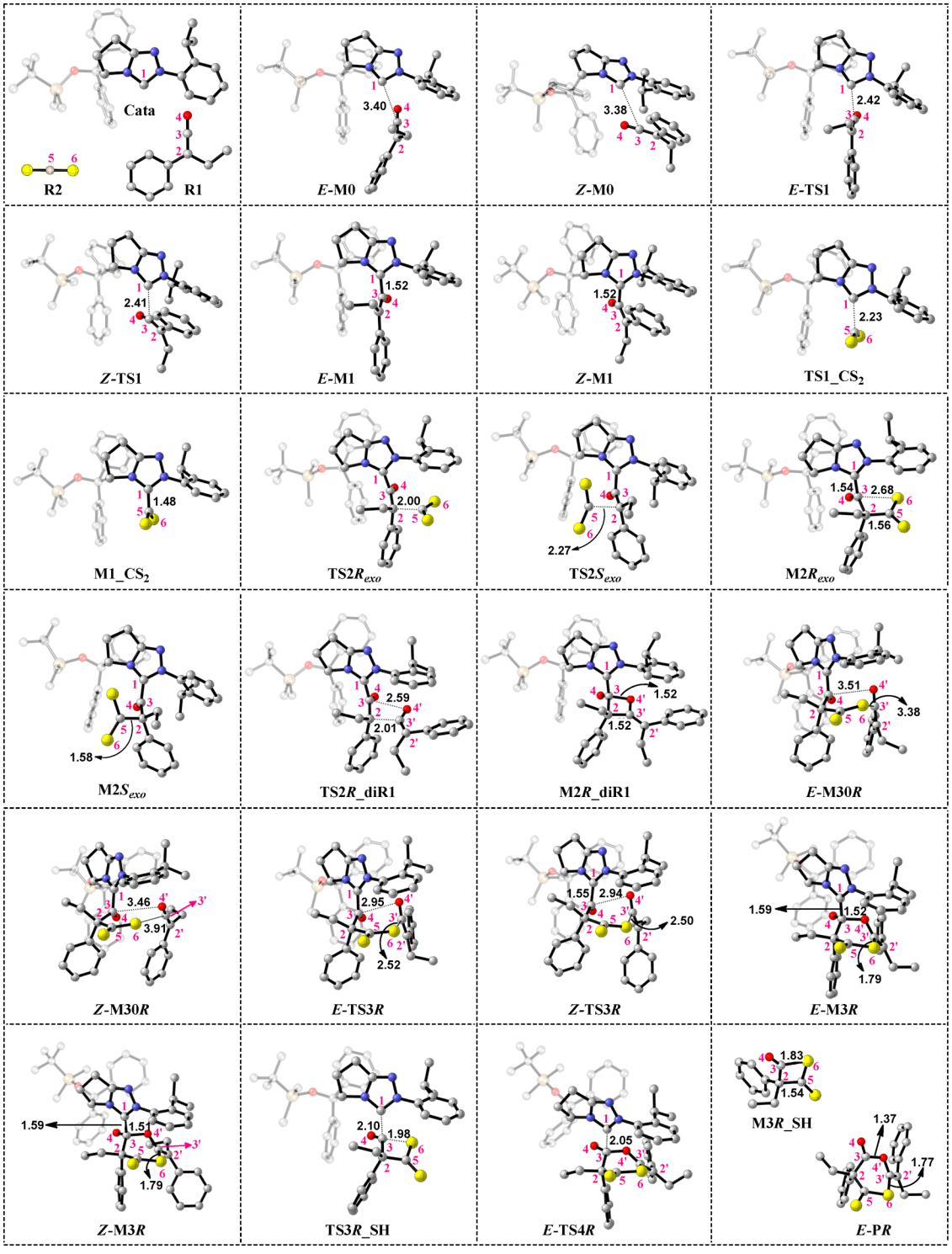

Figure 1. Optimized geometries of all the stationary points involved in the NHC-catalyzed reaction mechanism. All geometries are calculated by method A. All hydrogen atoms are omitted, the substituent groups $-C(Ar^1)_2OR$ of **Cata** are shown as transparent groups, and bond lengths are given in angstroms.

cycloaddition,[22] we have demonstrated that it is the ketene that NHC reacts with to start the cylcoaddition of ketene and diazenedicarboxylates. Tang et al.[24] have also found the "ketene-first" mechanism is exclusively more favorable to the "imine-first" catalytic cycle in the Staudinger reaction ([2 + 2] cycloaddition of a ketene with an imine). However, our previous study on NHC-catalyzed ketene [4 + 2] cyclo-addition[23] has verified that the "ketene-first" mechanism is unfavorable in comparison with the "diazene-first" mechanism. In experiments, Sereda et al.[25] have reported that the NHC–CS_2 adducts can be isolated at room temperature, whereas Ye et al.[10] clarify that no reaction happens between **Cata** and CS_2 under −40 °C (channel 1b in Scheme 3) and even the NHC–CS_2 adduct **M1_CS$_2$** (depicted in Scheme 3) cannot be converted to the final six-membered (sulfur, oxygen) heterocyclic product ***E*-PR** (depicted in Scheme 3). They

dx.doi.org/10.1021/jo4018809 | J. Org. Chem. 2013, 78, 11849−11859

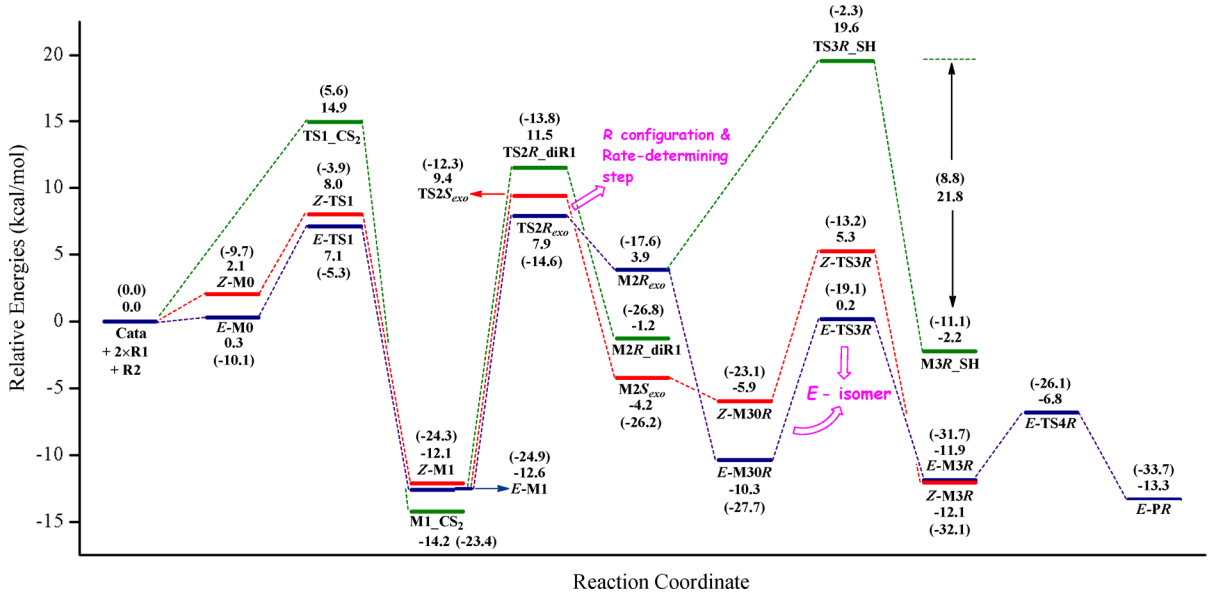

Figure 2. Free energy profiles of the NHC-catalyzed reaction mechanisms. Numbers in parentheses are relative Born−Oppenheimer energies. All energies (in kcal/mol) are calculated by method C.

thus conclude that the initial step of this title reaction should be the complexation of **Cata** with ketene **R1** (channel 1a) rather than CS_2 **R2** (channel 1b). Considering this specific reaction and experiment conditions, we tend to agree with channel 1a. In spite of this, here in the present study, we will give the computational results using density functional theory (DFT)[26] for both of these two possible reaction mechanisms to illustrate the theoretical methodology for this issue at the molecular level.

In addition, Lv and co-workers[27] have reported that NHCs can catalyze the asymmetric dimerization of ketene **R1** to yield lactone **diR1** at room temperature with THF as the solvent (channel 2a, Scheme 3), but we have no idea whether this dimerization would happen under the experimental conditions of the title reaction (at −40 °C with toluene as the solvent). In contrast, if the first step is verified to be **Cata** with **R2** through channel 1b, then this dimerization mechanism would be automatically excluded.

To the best of our knowledge, there as yet is no conclusive evidence about how CS_2 is added to this [2 + 2 + 2] catalytic cycle, but one can get some enlightenment from the experimental results[10] catalyzed by another Lewis base—*N*,*N*-dimethylpyridin-4-amine (DMAP, denoted as **Cata_D**) at −40 °C, which promotes the reaction of **R1** with **R2** to afford a mixed product of the four-membered sulfur heterocycle **M3*R*_SH** ([2 + 2] cycloadduct, Scheme 3) and the [2 + 2 + 2] cycloadduct ***E*-PR**. Furthermore, **M3*R*_SH** has been found to be able to react with one more molecule of **R1** with the presence of **Cata** to give ***E*-PR** under exactly the same conditions with the title reaction. Then what happens under the **Cata**-catalyzed conditions? Is it possible for (*E*/*Z*)-**M1** to react with CS_2 in the second step (channel 2b)? Will the [2 + 2] cycloaddition of ketene and CS_2 occur (channel 3b)? How is **M3*R*_SH** transformed to the [2 + 2 + 2] cycloaddition product ***E*-PR**? What are the differences between NHC-catalyzed and DMAP-catalyzed [2 + 2 + 2] cycloaddition mechanisms?

With all these questions as motivation, the present work will pursue a DFT theoretical investigation toward the title reaction in order to shed light on the details of each elementary step at the molecular level and to reach more comprehensive understanding of this interesting multimolecular cycloaddition. Although all those present available control experiments are indeed helpful for accessing some information about the reaction mechanisms, computational methods are in some sense, more effective and intuitionistic due to the limitation of experimental technologies for detecting intermediates and transition states.

2. COMPUTATIONAL DETAILS

All theoretical calculations were performed using the Gaussian 09 program,[28] with density functional theory (DFT) which has been widely utilized in the study of reaction mechanisms.[29,30] All structures of the reactants, products, transition states, and intermediates were optimized using the M06-2X[31] density functional along with the 6-31G*[32−34] basis set in the gas phase. The frequency calculations were performed at the same level at 233.15 K and 1 atm, which are exactly the same conditions as experiments,[10] in order to characterize that all minima structures have no imaginary frequency and all transition states have one and only one imaginary frequency. The same level of intrinsic reaction coordinate (IRC) calculations[35,36] was performed to ensure that each transition state leads to the expected reactants and products, and natural bond orbital (NBO) analyses were carried out to assign the atomic charges.[37−39]

On the basis of the optimized structures in the gas phase at the M06-2X/6-31G* level, the energies were then refined by M06-2X/6-311+G**[40−42] single-point calculations with solvent effects (toluene, which was chosen from the available experiment[10]) included and simulated by the IEFPCM[43,44] model. The zero-point energies (ZPEs) and thermal corrections to free energies calculated at the M06-2X/6-31G* level in the gas phase were used to approximate those values of geometries optimized at the M06-2X/6-311+G** level with solvent included. In the rest of this paper, we will denote the computational method of geometry optimization at the M06-2X/6-31G* level in gas phase as method A, geometry optimization at the M06-2X/6-311+G** level with solvent included as method B, and energy refinement with single-point energy calculated at the M06-2X/6-311+G** level with solvent included plus ZPE or thermal correction calculated at the M06-2X/6-31G* level in the gas phase as method C.

All discussions in this paper are based on geometries calculated by method A and Gibbs free energies predicted by method C. Although in our study and previous studies by others[23,45] this strategy of using

dx.doi.org/10.1021/jo4018809 | J. Org. Chem. 2013, 78, 11849−11859

geometries optimized in the gas phase and refined energies by single-point calculations at a higher level with solvent included has been verified to be suitable, here in the present study, a simple test is carried out for further confirmation: we first reoptimized structures of **Cata**, **R2**, **M1_CS$_2$**, and **TS1_CS$_2$** using method B, and then we compared the predictions of some key geometry parameters and the Gibbs free energies with those calculated by methods A and C, respectively. All results are provided in part 2 of the Supporting Information, where one can observe that the geometries of the selected stationary points optimized in solvent (method B) have tiny differences with those in gas phase (method A); the energy barriers calculated by methods B and C are consistent, with a deviation of 0.1 kcal/mol, and the relative free energies differ by no more than 0.4 kcal/mol.

We chose to make discussions based on Gibbs free energies rather than Born−Oppenheimer energies, which are the electronic (including nuclear-repulsion) energies plus ZPEs, because Born−Oppenheimer energies are independent of temperature. However, it is necessary to state that the entropic penalty in thermal corrections based on the ideal gas-phase model are often overestimated because the suppressing effects of the solvent and pressure on the translational and rotational degrees of freedom of the reactants cannot be properly accounted for by the gas-phase model.[46,47]

3. RESULTS AND DISCUSSION

As mentioned above, there are generally four steps in the proposed mechanism for this reaction cycle catalyzed by **Cata** (Scheme 2), and more than one possible channel has been stated for each step except the fourth one (Scheme 3). Figure 1 shows all the optimized structures (calculated by method A) involved in this NHC-catalyzed reaction,[49] and Figure 2 presents the Gibbs free energy profiles along with the relative Born−Oppenheimer energies shown in parentheses. In the following parts of this section, we will give detailed discussions step by step.

3.1. First Step: Addition of Cata to R1. For a catalytic reaction, it is an important but usually challenging issue to make sure the catalyst will first exert its effects on which reactant, because answers may be different through various factors such as the specific structure of catalyst, the reactant counterparts, and the experimental conditions. As stated in the Introduction, NHCs have been verified to be able to combine with ketene to initiate the [2 + 2] cycloaddition,[22,24] but the isolated NHC−CS$_2$ adduct has been accessed at room temperature as noted in the report of Sereda and co-workers.[25] It is worth noting that Ye and co-workers gave a quite careful control experiment study which clarified that no reaction between **Cata** and CS$_2$ occurs at −40 °C, and the NHC−CS$_2$ adduct cannot be converted to the final [2 + 2 + 2] cycloadduct. They thus concluded that the initial reaction should be combination of **Cata** with ketene **R1** (channel 1a) rather than with **R2** (channel 1b). With regard to this specific reaction, we are more likely to support the "ketene-first" mechanism. Nevertheless, in the present study, we carried out calculations on both of these two possible mechanisms with the temperature constricted to −40 °C to give a further confirmation of this issue with the computational methodology, which has been demonstrated to be an effective method to help figure out the most favorable mechanism.[22,23,29,48]

More details about channel 1a are given in Scheme 2: two precursor complexes, namely (*E*/*Z*)-**M0**, are first formed with the approach of **Cata** to **R1**; then the intermediates (*E*/*Z*)-**M1** are generated through the *exo* and *endo* attacks of the C1 atom in **Cata** at the C3 atom in **R1** via transition states (*E*/*Z*)-**TS1**, respectively. From channel 1b shown in Scheme 3, we can see that the C1 atom of **Cata** combines with the C5 atom of **R2** via transition state **TS1_CS$_2$** to form the intermediate **M1_CS$_2$**. The optimized geometries given in Figure 1 show that the distance between C1 and C3 atoms is shortened from 3.40/3.38 Å in (*E*/*Z*)-**M0** to 2.42/2.41 Å in (*E*/*Z*)-**TS1** and finally to 1.52/1.52 Å in (*E*/*Z*)-**M1**, while the distance between C1 and C5 atoms is shortened from 2.23 Å in **TS1_CS$_2$** to 1.48 Å in **M1_CS$_2$**, implying the full formation of the C1−C3 bond in NHC−ketene adducts (*E*/*Z*)-**M1** and the C1−C5 bond in the NHC−CS$_2$ adduct **M1_CS$_2$**, respectively.

In Figure 2, the Gibbs free energy barriers via transition states (*E*/*Z*)-**TS1** (7.1/8.0 kcal/mol) are found to be much lower than the barrier via **TS1_CS$_2$** (14.9 kcal/mol), which demonstrates that channel 1a occurs more favorably to initiate the reaction. This is consistent with the inference mentioned above. Nevertheless, the energy barrier of 14.9 kcal/mol to form the **M1_CS$_2$** adduct was not very high if the reaction was conducted at room temperature. This prediction offers a reasonable explanation to the experimental fact that NHC−CS$_2$ can be isolated at room temperature with the absence of ketene.[25] The agreement between experimental results and theoretical predictions demonstrates as well that the computational method utilized in the present work, including the density functional, basis set, and solvation model, is reasonable and reliable for the title reaction system. With regard to the stereoselectivity, as the free energy barrier difference via *E*-**TS1** (7.1 kcal/mol) in comparison to that via *Z*-**TS1** (8.0 kcal/mol) is predicted to be a value that lies within the error bar of the computational method, it is difficult to determine whether *E*-**M1** or *Z*-**M1** is preferred to be produced in the first step.

3.2. Second Step: Reaction Between (*E*/*Z*)-M1 and R2. *3.2.1. Reaction Patterns.* Similarly to the first step of the title reaction, there are also two possibilities for the second elementary step: (*E*/*Z*)-**M1** reacts with **R2** (channel 2b, Scheme 3) or with a second molecule of **R1** (channel 2a, Scheme 3). However, before we start to discuss the detailed mechanisms, we need to illustrate that there exist four possible reaction patterns (Table 1) for channel 2b, because for either

Table 1. Possible Reaction Patterns for Addition of R2 (Channel 2b) in the Second Step

possible reaction patterns in channel 2b	configuration of **M1**	added face of **M1**	chirality of C2 atom
R_{exo}	*E*	*Re*	*R*
R_{endo}	*Z*	*Re*	*S*
S_{exo}	*E*	*Si*	*S*
S_{endo}	*Z*	*Si*	*R*

E-**M1** or *Z*-**M1**, **R2** can attack from either their *Re* (denoted respectively as the R_{exo} and R_{endo} patterns) or *Si* face (denoted respectively as the S_{exo} and S_{endo} patterns) to participate in the reaction. All four of these reaction patterns have been investigated. The corresponding results including the free energy potential profiles of the four reaction patterns, and the optimized geometries of **TS2S_{endo}**, **TS2R_{endo}**, **M2S_{endo}**, and **M2R_{endo}** are provided in part 3 of the Supporting Information, where we can observe that the more energetically favorable pathways corresponding to the *R* configuration adduct and *S* configuration adduct are respectively reactions via transition states **TS2R_{exo}** and **TS2S_{exo}**, both of which refer to reactions of *E*-**M1** with **R2**. Here please note that we name all the transition states and adducts involved in channel 2b after denotations of the reaction patterns. Therefore, according to the definitions

dx.doi.org/10.1021/jo4018809 | J. Org. Chem. 2013, 78, 11849−11859

given in Table 1, all stationary points with a name ending in R_{exo} or S_{endo} correspond to those structures with an *R* chirality and all stationary points with a name ending in S_{exo} or R_{endo} correspond to those structures with an *S* chirality.

In channel 2a, in particular the dimerization of **R1**, the possible reaction patterns can be doubled, as **R1** can react by *exo* or *endo* attack at (*E*/*Z*)-**M1** to form the *E* or *Z* isomers associated with the configuration of the carbon double bond C2′═C3′ in **M2*R*_diR1**. In the present study, we calculate only one pattern of the eight which corresponds to the dominant configuration (*R* and *E* favorable) of **diR1** that is revealed by experimental results.[27] The other reaction patterns were left out from our computations on account of three reasons: (1) channel 2a is a competitive side reaction of the title [2 + 2 + 2] cycloaddition and so it is unnecessary to be our focus to discuss its stereoselectivities in detail, (2) the selected computational method, including the density functional, basis set, and solvation model, is verified to be able to predict the right stereoselectivities for this title reaction system (see the computational results in sections 3.2.2 and 3.3), and (3) the calculated results show that this investigated reaction pattern which corresponds to the experimentally predicted dominant configuration of **diR1** is much less favorable than that of channel 2b (see the computational results in section 3.2.2). Therefore, we believe it is reasonable to omit all other possible reaction patterns involved in channel 2a.

3.2.2. Reaction Mechanism. The transition state of the reaction between ***E*-M1** and **R1** through channel 2a is denoted as **TS2*R*_diR1** and that of the reaction between ***E*-M1** and **R2** through channel 2b as **TS2**$(R/S)_{exo}$. As displayed in Figure 1, the C2−C3′ and C3−O4′ bond lengths are shortened from 2.01 and 2.59 Å in **TS2*R*_diR1** to both being 1.52 Å in **M2*R*_diR1**, while the distance between the C2 and C5 atoms is decreased from 2.00/2.27 Å in **TS2**$(R/S)_{exo}$ to 1.56/1.58 Å in **M2**$(R/S)_{exo}$, respectively. That is, channel 2a follows the concerted mechanism to form the four-membered ring O4′−C3′−C2−C3 in **M2*R*_diR1** (Scheme 3), while in channel 2b, bonding between the C2 and C5 atoms occurs and results in intermediates **M2**$(R/S)_{exo}$ (Scheme 2), depending on the *Re* or *Si* face of ***E*-M1** that **R2** attacks. The free energy profile in Figure 2 shows that the transition state **TS2*R*_diR1** (11.5 kcal/mol) is located higher than **TS2**$(R/S)_{exo}$ (7.9/9.4 kcal/mol), indicating that ***E*-M1** reacts more favorably with **R2** to form **M2**$(R/S)_{exo}$ (channel 2b) rather than with another molecule of **R1** to form the dimeric product **M2*R*_diR1** (channel 2a). With regard to the enantioselectivity, it is easy to observe that the energy barrier via **TS2**R_{exo} (20.5 kcal/mol, associated with the *R* configuration) is lower than that via **TS2**S_{exo} (22.0 kcal/mol, associated with the *S* configuration), which indicates the preference to form the *R* configuration adduct **M2**R_{exo} in this step.

Although the reverse reaction barrier from **M2**R_{exo} back to ***E*-M1** turns out to be quite low at only 4.0 kcal/mol, the immediate combination of **M2**R_{exo} with a second molecule of **R1** in the following step will generate the very low energy complexes (*E*/*Z*)-**M30*R*** (−10.3/−5.9 kcal/mol). This helps to transform **M2**R_{exo} instantly, instead of leaving it to return back to ***E*-M1** along the reverse direction. Combining those discussions with what has been provided in part 3 in the Supporting Information, we conclude that channel 2b is more energetically favorable than channel 2a, and in channel 2b the R_{exo} reaction pattern is the most probable, which predicts a dominant *R* configuration of the C2 chiral center. All of these predictions are in good agreement with the experimental results.[10]

3.3. Third Step: Ring-Closure Reaction (Formally [4 + 2] Cycloaddition). As is shown in Scheme 2, since **M2**R_{exo} has been formed in the second step, the following step is to construct the six-membered (sulfur, oxygen) heterocycle that is included in the final product, which obviously needs to add another molecule of **R1** (channel 3a, Scheme 3), excluding the possibility of involving another molecule of **R2**. The NBO analysis shows that the negative charges are populated on the S6 atom (−0.181 e) in **M2**R_{exo} but positive charges on the C3′ atom (0.731 e) in **R1**, while in contrast the positive charges are assigned to the C3 atom (0.541 e) in **M2**R_{exo} but negative charges to the O4′ atom (−0.442 e) in **R1**. With the approach of **M2**R_{exo} to the second **R1** molecule, the electrostatic attraction between C3′ and S6 along with that between C3 and O4′ will lead to complexes in either an *E* or *Z* configuration (denoted as (*E*/*Z*)-**M30*R***), depending on which face of **R1** that **M2**R_{exo} gets close to. Subsequently, the six-membered ring is formed in (*E*/*Z*)-**M3*R*** via transition states (*E*/*Z*)-**TS3*R***, respectively. The IRC calculated results indicate that two bonds, i.e. C3′−S6 and C3−O4′, are formed by a concerted but not synchronous mechanism and their bond lengths are shortened from 3.38/3.91 and 3.51/3.46 Å in (*E*/*Z*)-**M30*R*** to 2.52/2.50 and 2.95/2.94 Å in (*E*/*Z*)-**TS3*R*** and finally to 1.79/1.79 and 1.52/1.51 Å in (*E*/*Z*)-**M3*R***, separately (Figure 1). The free energy profiles in Figure 2 show that ***E*-M30*R*** is located 4.4 kcal/mol lower than ***Z*-M30*R***, which implies that ***E*-M30*R*** will be the significantly dominant isomer from the aspect of thermodynamics. In addition, the energy barriers via ***E*-TS3*R*** and ***Z*-TS3*R*** are 10.5 and 11.2 kcal/mol, respectively, which also supports the preference to form the *E* isomer of the product. This prediction is consistent with the experimental fact that only the *E* isomer product can be detected.[10]

Even though the participation of a second molecule of **R2** is excluded, the intramolecular cyclization (channel 3b, Scheme 3) through bonding of atoms C3 and S6 may occur to compete with the intermolecular [4 + 2] cycloaddition stated above (channel 3a, Scheme 3). The experimental results of Ye and coworkers[10] show that with the Lewis base DMAP (denoted as **Cata_D**) as catalyst, the four-membered-ring sulfur heterocycle compound **M3*R*_SH** can be obtained under exactly the same experimental conditions as the title reaction (at −40 °C with toluene as the solvent). Herein, it would be very interesting and also crucial to see whether this can possibly happen using **Cata** as the catalyst.

The computational results predict that, in channel 3b, the intramolecular ring-closure reaction (formation of the C3−S6 bond) proceeds in a concerted step with the regeneration of **Cata** (breaking of the C1−C3 bond) via transition state **TS3*R*_SH** (Scheme 3). The changes in optimized geometry parameters (Figure 1) from **M2**R_{exo} to **TS3*R*_SH** and finally **M3*R*_SH** illustrate this process: the C1−C3 bond length is increased from 1.54 Å in **M2**R_{exo} to 2.10 Å in **TS3*R*_SH**, while the C3−S6 bond is shortened from 2.68 Å in **M2**R_{exo} to 1.98 Å in **TS3*R*_SH** and finally to 1.83 Å in **M3*R*_SH**, which indicates the full formation of the C3−S6 bond. From the energy profiles shown in Figure 2, it is easy to observe that the barrier through this intramolecular cyclization mechanism (15.7 kcal/mol) is much higher than that through the aforementioned intermolecular [4 + 2] cycloaddition mechanism (10.5/11.2 kcal/mol via (*E*/*Z*)-**TS3*R***, respectively). Therefore, in the third step, channel 3a is more energetically favorable than channel 3b.

dx.doi.org/10.1021/jo4018809 | J. Org. Chem. 2013, 78, 11849−11859

Scheme 4. Proposed Reaction Mechanisms of the Title Reaction Catalyzed by Cata_D

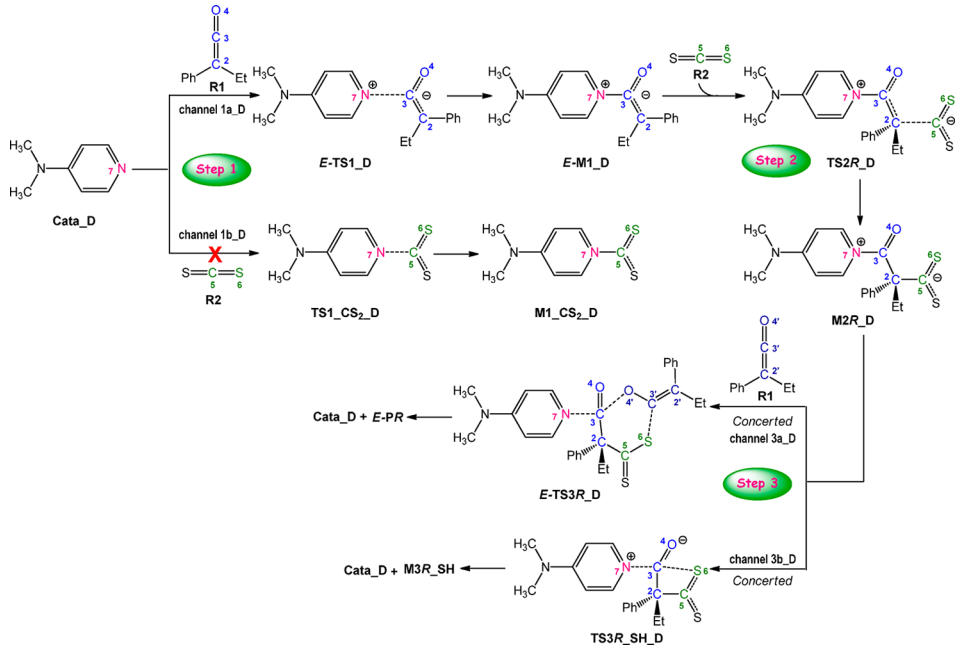

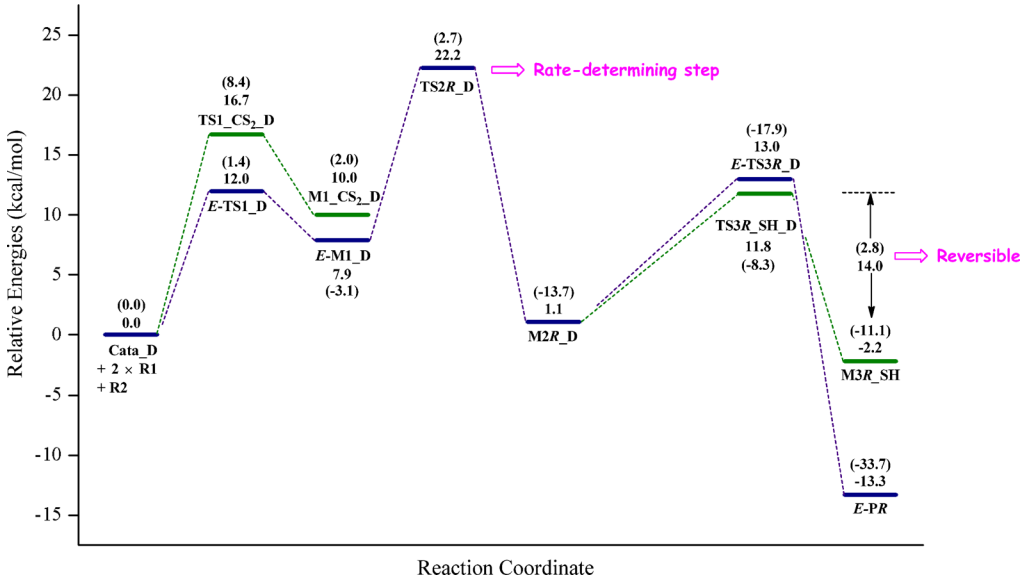

Figure 3. Free energy profiles of the DMAP-catalyzed reaction mechanism. Numbers in parentheses are relative Born−Oppenheimer energies. All energies (in kcal/mol) are calculated by method C.

Furthermore, the reverse reaction barrier from **M3*R*_SH** back to **M2*R*$_{exo}$** via **TS3*R*_SH** is 21.8 kcal/mol, which is close to that from ***E*-M1** to **M2*R*$_{exo}$** via **TS2*R*$_{exo}$** in the second step (20.5 kcal/mol). This observation probably offers a reasonable explanation for the experimental fact[10] that if one uses **M3*R*_SH** and ketene **R1** as the beginning reactants, the NHC catalyst can help to transform this sulfur heterocycle compound into the final product ***E*-PR**, which is predicted to go first to **M2*R*$_{exo}$** and then through channel 3a in the third step and the following fourth step.

3.4. Fourth Step: Regeneration of the Catalyst. Since in the third step the *E* isomer (***E*-M3*R***) has been validated to be the dominant [2 + 2 + 2] cycloadduct, here for the fourth step, we will perform calculations regarding this particular isomer only. The transition state of this step is denoted as ***E*-TS4*R***. As is shown in Figure 1, the C1−C3 bond length is increased from 1.59 Å in ***E*-M3*R*** to 2.05 Å in ***E*-TS4*R***, and the energy barrier of this step is only 5.1 kcal/mol, which indicates that the catalyst is easy to regenerate.

Taking all the four steps of the title reaction catalyzed by **Cata** into consideration, the more favorable mechanisms for the first three steps are respectively channel 1a, channel 2b, and channel 3a. The second step, i.e. addition of **R2**, is the rate-determining step of the whole reaction. It also determines the enantioselectivities (*R* favorable) associated with the chiral carbon C2 atom. In addition, the third step determines the other dominant stereoselective configuration (*E* favorable) related to the carbon double bond (C2′═C3′) in the [2 + 2 + 2] cycloaddition product.

dx.doi.org/10.1021/jo4018809 | J. Org. Chem. 2013, 78, 11849−11859

3.5. Reaction Mechanisms Catalyzed by Cata_D. In addition to the NHC-catalyzed reaction of **R1** with **R2**, the experimental results[10] also show the abilities of another Lewis base, DMAP (denoted as **Cata_D**), to catalyze **R1** to react with **R2** and generate both the [2 + 2] and [2 + 2 + 2] cycloadducts (**M3*R*_SH** and ***E*-PR**), but poorer yields are obtained. To clarify the cycloaddition mechanisms promoted by both **Cata** and **Cata_D** would be of help in exploring sources of their better or worse catalytic abilities. Therefore, we also carried out a brief mechanistic study on DMAP-catalyzed [2 + 2] and [2 + 2 + 2] cycloadditions.

Scheme 4 gives more details of the proposed DMAP-catalyzed reaction mechanism. Since it has been determined that the density functional and basis set used in this present study predict stereoselectivities exactly identical with the experimental results in the reaction catalyzed by **Cata**, here for the reaction promoted by **Cata_D**, we will make focus on only the dominant configuration of each step. For example, only the *E* isomer of the DMAP−ketene adduct ***E*-M1** is presented in the first step. Figure 3 shows the corresponding free energy profiles, and Figure 4 displays all the involved geometries optimized by method A,[49] except those common ones that have been shown in Figure 1.

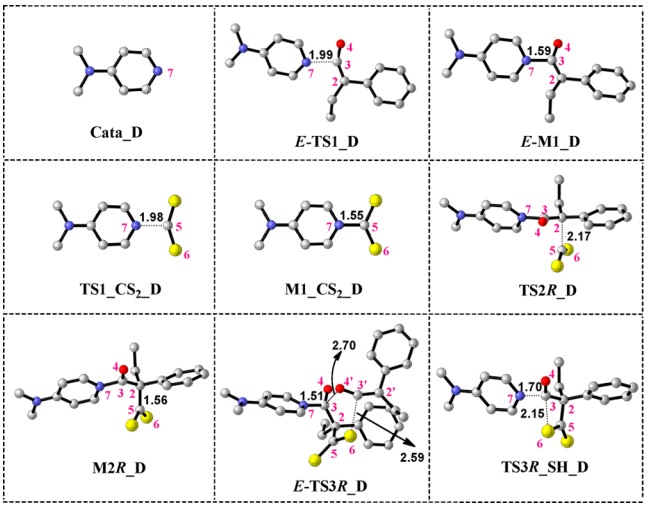

Figure 4. Optimized geometries of the stationary points involved in the DMAP-catalyzed reaction mechanism. All geometries are optimized by method A. All hydrogen atoms are omitted; bond lengths are given in angstroms.

The calculated results show that the energetically preferred mechanisms include three reaction steps: the reaction of **Cata_D** with **R1** via ***E*-TS1_D** to generate ***E*-M1_D** (channel 1a_D), the addition of **R2** to ***E*-M1_D**, and formal [4 + 2] cycloaddition concerted with regeneration of **Cata_D** (channel 3a_D). For the first step, the reaction of catalyst with **R2** (channel 1b_D) is excluded according to the energy barrier via **TS1_CS$_2$_D** (16.7 kcal/mol) being obviously higher than that via ***E*-TS1_D** (12.0 kcal/mol).

For the second step, in particular the combination of ***E*-M1_D** with **R2** through bonding of C2 and C5 atoms via transition state **TS2*R*_D**, the energy barrier is 14.3 kcal/mol, and the distance between C2 and C5 atoms is shortened from 2.17 Å in **TS2*R*_D** to 1.56 Å in **M2*R*_D**, indicating the full combination of **R2** with ***E*-M1_D**.

The third step is the concerted step of ring closure (formally [4 + 2] cycloaddition) and regeneration of **Cata_D** via transition state ***E*-TS3*R*_D** (channel 3a_D in Scheme 4). The distances between C3 and O4′, S6 and C3′, and N7 and C3 atoms in ***E*-TS3*R*_D** are 2.70, 2.59, and 1.51 Å, respectively (Figure 4). The energy barrier of this step is 11.9 kcal/mol, which is easily to be overcome under the experimental conditions.

We also checked the intramolecular cyclization through bonding of atoms C3 and S6 to yield the sulfur heterocycle **M3*R*_SH** via transition state **TS3*R*_SH_D** (channel 3b_D in Scheme 4). This is demonstrated to be accomplished in a concerted step as well, with the regeneration of **Cata_D**. As we can see from Figure 3, the free energy barriers via **TS3*R*_SH_D** in channel 3b_D (10.7 kcal/mol) is 1.2 kcal/mol lower than that via ***E*-TS3*R*_D** in channel 3a_D, indicating the preference to generate the [2 + 2] cycloadduct **M3*R*_SH**. This theoretical prediction accounts for the experimental fact of access to isolation of **M3*R*_SH**, but it seems to be inconsistent with the results that higher yield of the [2 + 2 + 2] cycloadduct (52%) in comparison to that for the [2 + 2] cycloadduct (10%) occurs when the reaction is promoted by **Cata_D** (Scheme 3).[10] Further observation shows that the energy barrier of the reverse reaction of channel 3b_D via **TS3*R*_SH_D** back to **M2*R*_D** (14.0 kcal/mol) is very easily overcome under the experimental conditions,[10] and ***E*-PR** (−13.3 kcal/mol) is located much lower than **M3*R*_SH** (−2.2 kcal/mol). Therefore, when the reaction system reaches its equilibrium, the final product could probably be expected to be a mixture of **M3*R*_SH** with ***E*-PR**, and it has a significant potential to contain a higher content of ***E*-PR**. However, for the NHC-catalyzed reaction, the transition state **TS3*R*_SH**, which corresponds to the intramolecular cyclization (channel 3b), is located as much as 19.4 kcal/mol (Figure 2) higher than ***E*-TS3*R***, which corresponds to the more favorable intermolecular [4 + 2] cycloaddition (channel 3a); therefore, isolation of **M3*R*_SH** is a remote possibility. However, if **M3*R*_SH** is initially added to the mixture of **R1** and **Cata**, it could go through the reverse reaction mechanism via **TS3*R*_SH** to form compound **M2*R*$_{exo}$** and then follow the remaining steps of the [2 + 2 + 2] reaction mechanism shown in Scheme 2. This conclusion is obtained on the basis of the energy barrier of the reverse reaction (21.8 kcal/mol) being comparable to that of the rate-determining step via **TS2*R*$_{exo}$** (20.5 kcal/mol). In a word, the DMAP-catalyzed reaction is more likely to generate the mixed products of **M3*R*_SH** and ***E*-PR**, but the NHC-catalyzed reaction tends to give only ***E*-PR** in higher yield. All these results are in good agreement with the experimental results.[10]

Further, the reaction mechanism of the unctalyzed [2 + 2 + 2] cycloaddition of **R1** and **R2** has also been studied to confirm the necessity of using catalysts. All these results and discussions are given in the Appendix.

4. CONCLUSIONS

The first DFT study toward the detailed reaction mechanisms of stereoselective [2 + 2 + 2] multimolecular cycloaddition of two molecules of ketene and one molecule of carbon disulfide (CS_2) catalyzed by an N-heterocyclic carbene (NHC) has been presented in this paper. The reaction is demonstrated to occur through four elementary steps, and for each of the first three steps, more than one possible channel that involves different participating molecules has been investigated. The calculated results reveal that the most favorable pathway contains four

dx.doi.org/10.1021/jo4018809 | J. Org. Chem. 2013, 78, 11849−11859

Scheme 5. Proposed Mechanism of the Uncatalyzed [2 + 2 + 2] Cycloaddition of R1 and R2

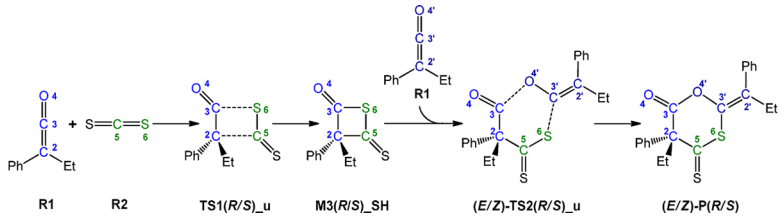

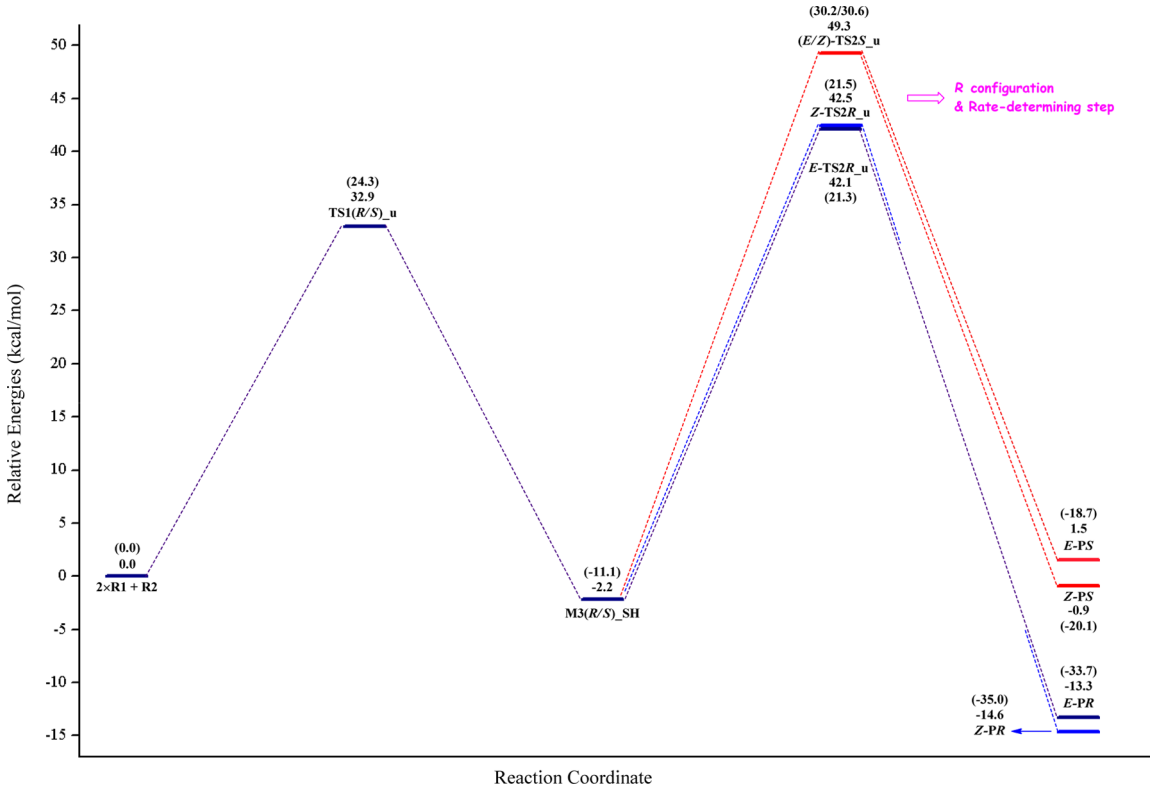

Figure 5. Free energy profiles of the proposed uncatalyzed [2 + 2 + 2] cycloaddition mechanism. Numbers in parentheses are relative Born–Oppenheimer energies. All energies (in kcal/mol) are calculated by method C.

elementary steps: the NHC catalyst first reacts with ketene **R1** to initiate the reaction (via channel 1a), then **R2** is added to the afore formed intermediate ***E*-M1** (via channel 2b), subsequently, another molecule of **R1** is involved in the third step to accomplish the ring closure (formally [4 + 2] cycloaddition, via channel 3a), and in the final step, the NHC catalyst is regenerated and the [2 + 2 + 2] cycloaddition product ***E*-PR** is released. The second step is demonstrated to be the rate-determining step with a free energy barrier of 20.5 kcal/mol, and the stereoselectivities associated with the chiral carbon center (C2 atom) and the carbon double bond (C2′═C3′) in the product ***E*-PR** turn out to be determined in the second and third steps, respectively. Moreover, the reaction mechanism of this [2 + 2 + 2] cycloaddition catalyzed by another Lewis base, DMAP, has also been explored, which is demonstrated to be very likely to yield a mixed product of the [2 + 2] and [2 + 2 + 2] cycloadducts: i.e., **M3*R*_SH** and ***E*-PR**. Therefore, the NHC catalyst is recommended for this variety of reaction. All computational results are in good agreement with the experimental facts. The mechanistic insights obtained in the present study should be valuable for the design of more efficient NHC catalysts and/or reactions to achieve diverse stereoselective [2 + 2 + 2] cycloadditions with ketene and/or CS_2.

5. APPENDIX

The mechanism of the uncatalyzed [2 + 2 + 2] cycloaddition of two molecules of **R1** and one molecule of **R2** is researched to help clarify the necessity of using catalysts. Scheme 5 illustrates the details of the proposed reaction mechanism, and Figure 5 gives the Gibbs free energy profiles calculated by method C.

In the uncatalyzed cycloaddition mechanism, one molecule of **R1** reacts with **R2** via transition states **TS1(*R*/*S*)_u** to respectively form the two sulfur heterocycle compounds **M3(*R*/*S*)_SH**, depending on which face (*Re* or *Si*) of **R1** that **R2** attacks. With the approach of the second molecule of **R1**, the C3–S6 bond in **M3(*R*/*S*)_SH** is broken, and a formal [4 + 2] cycloaddition occurs to form the final product in either *E* or *Z* configuration which is associated with the double bond of C2′═C3′.

As we can see from the free energy profiles shown in Figure 5, the energy barriers via **TS1*R*_u** and **TS1*S*_u** are exactly the same at 32.9 kcal/mol. **M3*R*_SH** and **M3*S*_SH** have the same energy as well, which is 2.2 kcal/mol lower than that of the reactants. In the second step, the two transition states with *S*

dx.doi.org/10.1021/jo4018809 | J. Org. Chem. 2013, 78, 11849–11859

configuration, namely (*E*/*Z*)-**TS2*S*_u**, have exactly the same free energies of 49.3 kcal/mol and slightly different Born−Oppenheimer energies of 30.2/30.6 kcal/mol, respectively; the two transition states with *R* configuration, namely (*E*/*Z*)-**TS2*R*_u**, have different but quite similar free energy values of 42.1/42.5 kcal/mol and Born−Oppenheimer energies of 21.3/21.5 kcal/mol, respectively. These results indicate that the second step, in particular the formal [4 + 2] cycloaddition, identifies the dominant configuration (*R* favorable) that is associated with the chiral carbon center (C2 atom), and it is also the rate-determining step of the whole reaction. Obviously, the very high energy barriers via the second step of the uncatalyzed reaction, which range from 44.3 to 51.5 kcal/mol, indicate that this [2 + 2 + 2] cycloaddition could hardly occur under mild experimental conditions without the presence of catalysts. Moreover, although the enantioselectivity may be good, as both of the *R* configuration transition states ((*E*/*Z*)-**TS2*R*_u**) are located lower than the *S* configuration states ((*E*/*Z*)-**TS2*S*_u**), the stereoselectivity associated with the double bond C2′═C3′ could be very poor, which is due to the same barrier via ***E*-TS2*S*_u** and ***Z*-TS2*S*_u** (51.5 kcal/mol) or the quite similar barriers via ***E*-TS2*R*_u** and ***Z*-TS2*R*_u** (44.3 and 44.7 kcal/mol, respectively).

On the basis of discussions stated above, we conclude that some effective measures working to lower the energy barriers are very essential for the purpose of performing this [2 + 2 + 2] cycloaddition of **R1** and **R2** under mild conditions, and as we all know, the addition of a proper catalyst is quite a facile strategy.

■ ASSOCIATED CONTENT

Ⓢ Supporting Information

Text, tables, and figures giving Gibbs free energies (*G*) and Born−Oppenheimer energies (*E*) of all stationary points involved in this study (part 1), a test of the suitability of using single-point refined energies (part 2), enantioselectivity studies of channel 2b in the second step of NHC-catalyzed reaction mechanisms (part 3), and Cartesian coordinates of all structures (part 4). This material is available free of charge via the Internet at http://pubs.acs.org.

■ AUTHOR INFORMATION

Corresponding Authors

*E-mail for D.-H.W.: donghuiwei@zzu.edu.cn.

*E-mail for M.-S.T.: mstang@zzu.edu.cn.

Notes

The authors declare no competing financial interest.

■ ACKNOWLEDGMENTS

The work described in this paper was supported by the National Natural Science Foundation of China (No. 21303167), China Postdoctoral Science Foundation (No. 2013M530340), and Excellent Doctoral Dissertation Engagement Fund of Zhengzhou University in 2012.

■ REFERENCES

(1) Glorius, F. *N-Heterocyclic Carbenes in Catalysis-An Introduction*; Springer-Verlag: Berlin, Heidelberg, 2006; Vol. *21*, pp 1−20.

(2) Nolan, S. P. *Acc. Chem. Res.* **2010**, *44*, 91−100.

(3) Enders, D.; Niemeier, O.; Henseler, A. *Chem. Rev.* **2007**, *107*, 5606−5655.

(4) Glorius, F.; Hirano, K. Nucleophilic Carbenes as Organocatalysts. *Ernst Schering Foundation Symposium Proceedings*; Springer-Verlag: Berlin, Heidelberg, 2008; Vol. *2*, pp 159−181.

(5) Moore, J. L.; Rovis, T. *Top. Curr. Chem.* **2010**, *291*, 77−144.

(6) Tidwell, T. T. *Angew. Chem., Int. Ed.* **2005**, *44*, 5778−5785.

(7) Paull, D. H.; Weatherwax, A.; Lectka, T. *Tetrahedron* **2009**, *65*, 6771−6803.

(8) Wang, X.-N.; Shao, P.-L.; Lv, H.; Ye, S. *Org. Lett.* **2009**, *11*, 4029−4031.

(9) Huang, X.-L.; He, L.; Shao, P.-L.; Ye, S. *Angew. Chem., Int. Ed.* **2009**, *48*, 192−195.

(10) Wang, X.-N.; Shen, L.-T.; Ye, S. *Chem. Commun.* **2011**, *47*, 8388−8390.

(11) Douglas, J.; Taylor, J. E.; Churchill, G.; Slawin, A. M. Z.; Smith, A. D. *J. Org. Chem.* **2013**, *78*, 3925−3938.

(12) McCasland, G. E.; Zanlungo, A. B.; Durham, L. J. *J. Org. Chem.* **1974**, *39*, 1462−1466.

(13) Munday, R.; Zhang, Y.; Paonessa, J. D.; Munday, C. M.; Wilkins, A. L.; Babu, J. *J. Med. Chem.* **2010**, *53*, 4761−4767.

(14) Yamamoto, Y.; Takagishi, H.; Itoh, K. *J. Am. Chem. Soc.* **2001**, *124*, 28−29.

(15) Tanaka, K.; Wada, A.; Noguchi, K. *Org. Lett.* **2006**, *8*, 907−909.

(16) Kihara, N.; Nakawaki, Y.; Endo, T. *J. Org. Chem.* **1995**, *60*, 473−475.

(17) Shen, Y.-M.; Duan, W.-L.; Shi, M. *Eur. J. Org. Chem.* **2004**, *2004*, 3080−3089.

(18) Gabillet, S.; Lecerclé, D.; Loreau, O.; Carboni, M.; Dézard, S.; Gomis, J.-M.; Taran, F. *Org. Lett.* **2007**, *9*, 3925−3927.

(19) Wu, J.-Y.; Luo, Z.-B.; Dai, L.-X.; Hou, X.-L. *J. Org. Chem.* **2008**, *73*, 9137−9139.

(20) Yamamoto, Y.; Kinpara, K.; Saigoku, T.; Takagishi, H.; Okuda, S.; Nishiyama, H.; Itoh, K. *J. Am. Chem. Soc.* **2004**, *127*, 605−613.

(21) Clegg, W.; Harrington, R. W.; North, M.; Villuendas, P. *J. Org. Chem.* **2010**, *75*, 6201−6207.

(22) Wei, D.; Zhu, Y.; Zhang, C.; Sun, D.; Zhang, W.; Tang, M. *J. Mol. Catal. A: Chem* **2011**, *334*, 108−115.

(23) Zhang, W.; Zhu, Y.; Wei, D.; Li, Y.; Tang, M. *J. Org. Chem.* **2012**, *77*, 10729−10737.

(24) Tang, K.; Wang, J.; Cheng, X.; Hou, Q.; Liu, Y. *Eur. J. Org. Chem.* **2010**, *2010*, 6249−6255.

(25) Sereda, O.; Blanrue, A.; Wilhelm, R. *Chem. Commun.* **2009**, *0*, 1040−1042.

(26) Kohn, W. *Rev. Mod. Phys.* **1999**, *71*, 1253−1266.

(27) Lv, H.; Zhang, Y.-R.; Huang, X.-L.; Ye, S. *Adv. Synth. Catal.* **2008**, *350*, 2715−2718.

(28) Frisch, M. J.; Trucks, G. W.; Schlegel, H. B.; Scuseria, G. E.; Robb, M. A.; Cheeseman, J. R.; Scalmani, G.; Barone, V.; Mennucci, B.; Petersson, G. A.; Nakatsuji, H.; Caricato, M.; Li, X.; Hratchian, H. P.; Izmaylov, A. F.; Bloino, J.; Zheng, G.; Sonnenberg, J. L.; Hada, M.; Ehara, M.; Toyota, K.; Fukuda, R.; Hasegawa, J.; Ishida, M.; Nakajima, T.; Honda, Y.; Kitao, O.; Nakai, H.; Vreven, T.; Montgomery, J. A., Jr.; Peralta, J. E.; Ogliaro, F.; Bearpark, M.; Heyd, J. J.; Brothers, E.; Kudin, K. N.; Staroverov, V. N.; Kobayashi, R.; Normand, J.; Raghavachari, K.; Rendell, A.; Burant, J. C.; Iyengar, S. S.; Tomasi, J.; Cossi, M.; Rega, N.; Millam, J. M.; Klene, M.; Knox, J. E.; Cross, J. B.; Bakken, V.; Adamo, C.; Jaramillo, J.; Gomperts, R.; Stratmann, R. E.; Yazyev, O.; Austin, A. J.; Cammi, R.; Pomelli, C.; Ochterski, J. W.; Martin, R. L.; Morokuma, K.; Zakrzewski, V. G.; Voth, G. A.; Salvador, P.; Dannenberg, J. J.; Dapprich, S.; Daniels, A. D.; Farkas, Ö.; Foresman, J. B.; Ortiz, J. V.; Cioslowski, J.; Fox, D. J. *Gaussian 09, Revision C.01*; Gaussian, Inc., Wallingford, CT, 2010.

(29) Zhang, C.; Zhu, Y.; Wei, D.; Sun, D.; Zhang, W.; Tang, M. *J. Phys. Chem. A* **2010**, *114*, 2913−2919.

(30) Domingo, L. R.; Pérez-Ruiz, R. l.; Argüello, J. E.; Miranda, M. A. *J. Phys. Chem. A* **2009**, *113*, 5718−5722.

(31) Zhao, Y.; Truhlar, D. G. *Theor. Chem. Acc.* **2008**, *120*, 215−241.

(32) Hehre, W. J.; Ditchfield, R.; Pople, J. A. *J. Chem. Phys.* **1972**, *56*, 2257−2261.

(33) Hariharan, P. C.; Pople, J. A. *Theor. Chim. Acta* **1973**, *28*, 213−222.
(34) Francl, M. M.; Pietro, W. J.; Hehre, W. J.; Binkley, J. S.; Gordon, M. S.; DeFrees, D. J.; Pople, J. A. *J. Chem. Phys.* **1982**, *77*, 3654−3665.
(35) Gonzalez, C.; Schlegel, H. B. *J. Chem. Phys.* **1989**, *90*, 2154−2161.
(36) Gonzalez, C.; Schlegel, H. B. *J. Phys. Chem.* **1990**, *94*, 5523−5527.
(37) Reed, A. E.; Weinhold, F. *J. Chem. Phys.* **1983**, *78*, 4066−4073.
(38) Foster, J. P.; Weinhold, F. *J. Am. Chem. Soc.* **1980**, *102*, 7211−7218.
(39) Glendening, E. D.; Reed, A. E.; Carpenter, J. E.; Weinhold, F. *NBO Version 3.1*.
(40) Krishnan, R.; Binkley, J. S.; Seeger, R.; Pople, J. A. *J. Chem. Phys.* **1980**, *72*, 650−654.
(41) McLean, A. D.; Chandler, G. S. *J. Chem. Phys.* **1980**, *72*, 5639−5648.
(42) Clark, T.; Chandrasekhar, J.; Spitznagel, G. W.; Schleyer, P. v. R. *J. Comput. Chem.* **1983**, *4*, 294−301.
(43) Sang-Aroon, W.; Ruangpornvisuti, V. *Int. J. Quantum Chem.* **2008**, *108*, 1181−1188.
(44) Tomasi, J.; Mennucci, B.; Cancès, E. *J. Mol. Struct. (THEOCHEM)* **1999**, *464*, 211−226.
(45) Huang, F.; Zhang, C.; Jiang, J.; Wang, Z.-X.; Guan, H. *Inorg. Chem.* **2011**, *50*, 3816−3825.
(46) Huang, F.; Lu, G.; Zhao, L.; Li, H.; Wang, Z.-X. *J. Am. Chem. Soc.* **2010**, *132*, 12388−12396.
(47) Liang, Y.; Liu, S.; Xia, Y.; Li, Y.; Yu, Z.-X. *Chem. -Eur. J* **2008**, *14*, 4361−4373.
(48) Zhang, W.; Zhu, Y.; Wei, D.; Tang, M. *J. Comput. Chem.* **2012**, *33*, 715−722.
(49) Legault, C. Y. *CYLview, 1.0b*; Université de Sherbrooke, 2009 (http://www.cylview.org).